Pupil plane optimization for single-mode multi-axial optical interferometry with a large number of telescopes

J.-B. Le Bouquin, E. Tatulli

Mon. Not. R. Astron. Soc. **372,** 639–645 (2006) doi:10.1111/j.1365-2966.2006.10805.x

Pupil plane optimization for single-mode multi-axial optical interferometry with a large number of telescopes

J.-B. Le Bouquin[1,2]⋆ and E. Tatulli[2,3]

[1]*European Southern Observatory, Casilla 19001, Santiago 19, Chile*
[2]*Laboratoire d'Astrophysique, Observatoire de Grenoble, 38041 Grenoble, France*
[3]*Osservatorio di Arcetri, L.go E. Fermi, 5, 50125 Firenze, Italy*

Accepted 2006 July 12. Received 2006 July 7; in original form 2006 May 29

ABSTRACT

Future and planned optical long-baseline interferometers will allow rapid spectro-imaging at high angular resolution. A non-homothetic Fizeau instrument using optical fibres is one of the most promising concepts because it combines good sensitivity and high spectral resolution capabilities. However, when increasing the number of input telescopes, one critical issue is the design of the beam recombination scheme, at the heart of the instrument. Extending our previous analysis on the multi-axial 'all-in-one' recombination, where the beams are mixed all together, in this paper we tackle the possibility of reducing the number of pixels that are coding the fringes by compressing the pupil plane from a partially redundant output pupils configuration. Shrinking the number of pixels, which drastically increases with the number of recombined telescopes, is indeed a key issue that enables one to reach a higher limiting magnitude, but also allows one to lower the required spectral resolution and fasten the fringe reading process. By means of numerical simulations, we study the performances of existing estimators of the squared visibility with respect to the compression process. We show that not only does the model-based estimator lead to better signal-to-noise ratio (S/N) performances than the Fourier ones, but above all it is the only one that prevents the introduction of baseline mixing biases in the visibilities as the pupil plane compression rate increases. Furthermore, we show that moderate compression allows one to keep the S/N of the visibilities unaffected. In light of these conclusions, we propose an optimized pupil arrangement for six- and eight-beam recombiners.

Key words: instrumentation: interferometers – methods: data analysis – techniques: interferometric.

1 INTRODUCTION

After the first results of the Cambridge Optical Aperture Synthesis Telescope (COAST; Baldwin et al. 1996; Young et al. 2000), Navy Prototype Optical Interferometer (NPOI; Hummel 1998) and Infrared Optical Telescope Array (IOTA; Monnier et al. 2004b), the next challenge of optical long-baseline interferometry is to commonly perform spectro-imaging of faint sources. From the end of 2005, this technique has moved one step forwards with the operating of the Astronomical Multiple BEam Recombiner (AMBER) instrument (Petrov et al. 2003), the near-infrared combiner of the Very Large Telescope Interferometer (VLTI; Glindemann et al. 2003). However, with its three beams, it will require several nights to be able to restore consistent images (Thiébaut, Garcia & Foy 2003). Then, huge improvements are contemplated to be accomplished with second-generation instruments that will use four, six or even eight telescopes coupled with spectral resolution abilities (Malbet et al. 2004). One critical point in the design is the choice of the beam recombination concept, heart of the instrument.

The interferometric observables are the complex coherence factors (amplitude and phase) of the fringes formed by each pair of beams (the so-called baselines). They contain the information related to the spatial distribution of the source at high angular resolution. The simplest way to recover all the available information is to mix all the beams together (an all-in-one scheme), as their is no need to split and rearrange the beams as in a pairwise design. Besides, it leads to better performances in the photon noise regime, because *all photons* are used to create *all fringes*. Those fringes appear by modulating the optical path differences between the beams. That can be done temporally (with coaxial or Michelson modulation) or spatially (with multi-axial or Fizeau modulation). Comparing these two solutions, recent studies emphasized the advantages of the multi-axial concept thanks to fewer beam splitters, mirrors and outputs (LeBouquin et al. 2004a).

⋆E-mail: jlebouqu@eso.org

However, to measure the coherence factor of each baseline individually, the geometry of the multi-axial combiner has to be carefully checked. On the detector, each pair of pupils produces a fringe pattern with a frequency given by their separation. In order to separate the energy of each fringe pattern in the Fourier plane, the output pupil configuration should be *non-redundant*. This necessary condition can be achieved with bidimensional or linear arrangements. In the first approach, the focal image is fringed in different directions, while in the second one all fringes are aligned but use different frequencies. Only this last 1D diffraction pattern can be injected into a slit of the spectrograph, opening spectral abilities at medium and large resolutions. It explains why the majority of the projects only consider linearly aligned output pupils, like the VLTI Spectro Imager (VSI; Malbet et al. 2004), the Michigan Infrared Combiner (MIRC; Monnier et al. 2004a), the Multi Aperture Mid-Infrared Spectroscopic Experiment (MATISSE) and the Visible Spectrograph and Polarimeter (VEGA; Mourard, private communication).

From Monte Carlo simulations, Ribak et al. (1988) derived geometries allowing up to 30 beams to be combined without any redundancy. However, the number of frequencies dramatically increases with the number of input beams. For instance, 35 different frequencies are required for eight beams. Reducing this number has been initially proposed by Vakili & Koechlin (1989), for a visible interferometer in the presence of a fully turbulent image (dispersed fringed speckles). The authors used a *completely redundant* configuration but introduced small optical path differences to differently tilt the fringes in the dispersed image and thus separate the information. However, to save the spectral resolution abilities, the spectral dimension should be oversampled and the total number of pixels remains the same: the coding is converted from spatial to spectro-spatial. This method has never been used but could probably be explored to combine a large number of telescopes. Nevertheless, it is clearly beyond the scope of this paper, because it requires a global analysis taking into account its technical specificity (high spectral resolution, spectro-spatial coding). To fit with existing and future instrumentation, our work focuses on a *partially redundant* output pupils configuration, without using an optical path difference.

In this case, to be able to recover the interferometric quantities, the fringed image pattern should not be blurred by the atmospheric turbulence. In other words, the image should be stabilized and not contain moving speckles. Practically, the common way to transform a corrugated input wavefront into a planar and stable output is to spatially filter the beams with single-mode fibres. It also drastically improves the accuracy of the instrument as demonstrated by the Fiber Linked Unit for Recombination (FLUOR) experiment (Perrin 1997; Coudé Du Foresto et al. 1998) and theoretical studies (Tatulli, Mège & Chelli 2004). Yet, the average phase difference between the pupils (the so-called piston) should remain constant over the exposure time. This is ensured by freezing the random atmospheric piston with short exposures of a few milliseconds, or by the help of an external fringe tracker that allows longer exposures. However, this is not an issue for our study, because the same frame-to-frame data processing can be applied to both short or long exposures. Finally, the average value (distance to white fringe) and the residual motion (high frequency jitter) of the piston during each exposure will lead to contrast losses that have to be calibrated. Again, this pure multiplicative factor on the fringe amplitude has no incidence in our study.

All these advantages explain why *partially redundant multi-axial combination* and *spatial filtering* is the set-up currently used in the AMBER interferometer and also why it is a contemplated solution for next-generation instruments. Even so, no studies of the influence of the pupil redundancy on the interferometric quantities and on their estimators have been published. The objective of this work is to fill this gap. In Section 2, we present the description of the single-mode all-in-one multi-axial combination. We clarify the relation between the pupil and the interferogram planes. We explain why and how to reduce the maximum coding frequency of the fringes by compressing the pupil plane. We recall four different estimators of the squared visibility that can be used in the case of single-mode interferometry. In Section 3, these estimators are compared in terms of relative performance. We investigate how they are robust with respect to the compression process. Finally, Section 4 contains applications to future projects making use of the multi-axial all-in-one scheme with an increasing number of recombined beams. Thanks to results derived in previous sections, we propose an optimal output pupil configuration for six- and eight-beam combiners.

This work is the second part of our study of single-mode multi-axial combination for astronomical interferometry. The work presented here makes intensive use of the formalism and the results presented in the first paper (Paper I, Tatulli & LeBouquin 2006).

2 SINGLE-MODE MULTI-AXIAL COMBINATION

We redefine here only the parameters relevant for this part of the study. For a detailed description of the single-mode multi-axial combination, the reader can refer to Section 2 of Paper I. The different spatially filtered beams are superimposed in a focal plane, forming a fringed image. The amplitude and phase of this modulation, also called complex visibility, are related to the source intensity distribution at high angular resolution, by the Zernike van Cittert theorem. Strictly speaking, the visibility obtained with a fibred interferometer is not the source visibility but the so-called modal visibility (Mège 2003), which we will consider to be our observable.

Due to the spatial filtering, the shape of the image pattern and the fringe frequencies is completely defined by the width and the separation of the output pupils (Fig. 1). We called D the width of the beams in a pupil plane, here defined by the extension of the fibre mode. The fringes are weighted by the diffraction pattern of the fibre mode in the image plane (here Gaussian, dashed line in Fig. 1, top panel). The number of fringes in this pattern ($N_{\rm fri}$) is fixed by the distance between the output pupils. $N_{\rm pattern}$ is the detector reading window size expressed in units of the diffraction pattern, i.e. $N_{\rm pattern} = 1$ means half of the lobe of the Gaussian pattern has been considered. It also corresponds to the number of independent frequency points under each peak (Fourier sampling law). Additionally, P_i is a non-redundant integer list that fixes the relative positions of the other pupils and thus of the others peaks. Note that the largest frequency used in the Fourier plane identifies with the largest distance between two pupils. Thus, the position x_i of the pupils i (starting with $i = 0$ for the first one) can be expressed as

$$x_i = P_i \, N_{\rm fri} \, D, \tag{1}$$

where P_i is the non-redundant integer list,

$$P_i = (0, 1, 3), \tag{2}$$

$$P_i = (0, 1, 4, 6), \tag{3}$$

for three- (equation 2) and four-beam combiners (equation 3). With such assumptions, the peaks corresponding to each fringe pattern are equally spaced in the Fourier plane (Fig. 1, middle panel).

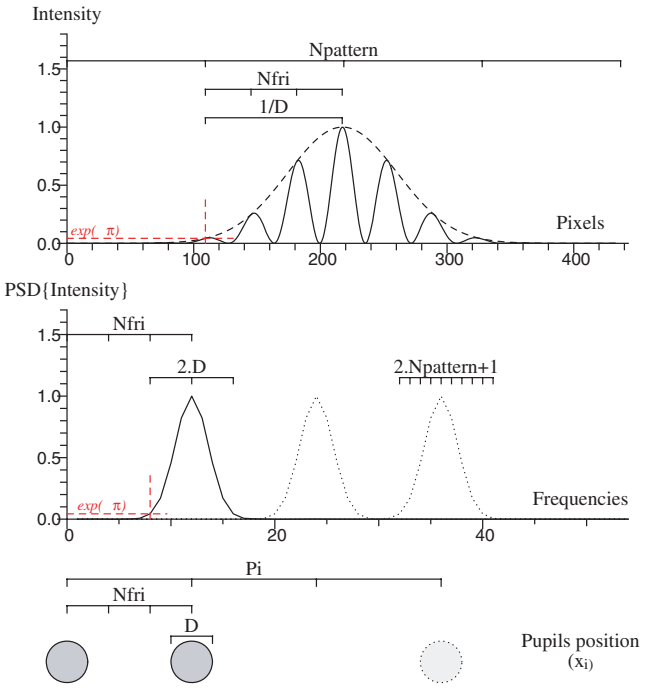

Figure 1. Geometrical relations between the image in the focal plane (top panel), its power spectral density (PSD; middle panel) and the output pupil configuration (bottom panel) of a multi-axial all-in-one single-mode interferometer. Here is shown a three-beam combiner when beam 1 and 2 are illuminated with an instrumental contrast set to 1. When beam 3 is illuminated, two other fringe systems appear (dotted lines in the Fourier space; the corresponding fringes in the image space have not been drawn for the sake of clarity). The displayed geometry is defined by $N_{\rm fri} = 3, N_{\rm pattern} = 4$ and $P_i = (0, 1, 3)$. See text for a complete explanation of these parameters.

2.1 Pupil plane compression

To separate the Fourier peaks, the distance between the pupils should be at least twice the pupil width ($N_{\rm fri} \geqslant 2$). When increasing the number of beams, the non-redundant configuration P_i reaches wide frequency ranges, such as 35 for an eight-beam combiner. Thus the largest distance between two pupils is $2 \times 35 = 70$ times the pupil width (equation 1). Using $N_{\rm pattern} \geqslant 2$ to record the whole image pattern, the number of fringes is $2 \times 35 \times 2 = 140$, and it requires about $2 \times 35 \times 2 \times 4 = 560$ pixels to sample them. At the same time, such a combiner requires a minimal spectral resolution of about 600, to be sure that the number of fringes in the coherence length is larger than the number of recorded fringes. First, reducing the frequency range reduces the number of pixels used to code the signal and thus the detector noise contribution. Besides, reducing the number of recorded fringe allows one to reduce the minimal spectral resolution, when the dispersion is not mandatory for the scientific case.

The first way to scale down the frequency range is to reduce $N_{\rm fri}$. It corresponds to a homothety of the pupil and the Fourier planes without changing the pupil diameter and peak width. Peaks start to overlap when $N_{\rm fri} < 2$, and the overlapping rate is similar for all of them. However, it is impossible to have $N_{\rm fri} < 1$ because the pupils cannot spatially overlap. As a result, this method has limited compression capability. Another solution to perform more efficient compression is to keep the distance between the first and second pupils fixed (i.e the $N_{\rm fri}$ parameter) and only rescale the position of the third and further pupils. If we conserve an homothetic scaling

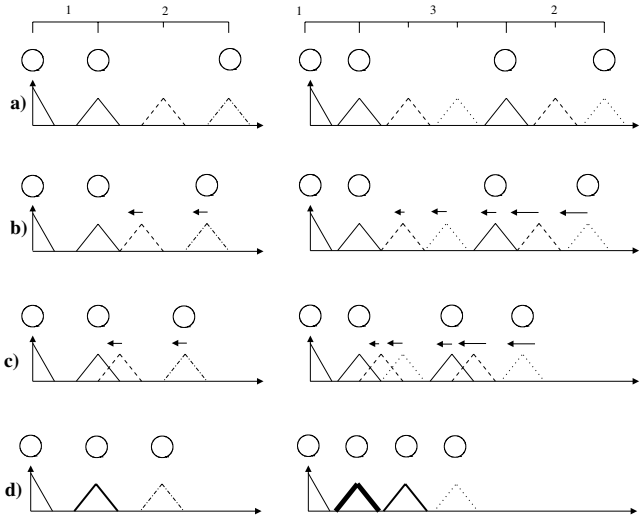

Figure 2. Superposition of the peak due to the compression of the pupil plane by equation (4) for three- and four-beam combiners. The compression factor is set to $\rho = 1, 2/N_{\rm fri}, 1/N_{\rm fri}$ and 0 (a, b, c and d).

of the latter (namely the compression factor ρ) to keep a partial non-redundancy, the positions of the pupils now follow

$$x_i = [i + (P_i - i)\rho]N_{\rm fri}\, D. \quad (4)$$

The smallest frequency does not shift, and the Fourier plane transformation is not perfectly homothetic. Gaps are created with a size of $N_{\rm fri}$, the original space unit between the pupils. Interesting values are displayed on Fig. 2 as follows.

(i) Panel (a): the pupils and Fourier peaks are at the positions defined by equation (1).

(ii) Panels (a) → (b): the Fourier peaks do not overlap each other, the configuration is not compressed.

(iii) Panels (b) → (c): the Fourier peaks overlap each other by less than a half and the configuration is *slightly compressed*.

(iv) Panels (c) → (d): the Fourier peaks overlap more than a half of the peak width and the configuration is *strongly compressed*.

(v) Panel (d): the pupil space is constant and the configuration is fully redundant. In the Fourier plane, the peaks are superposed by groups separated by $N_{\rm fri}$.

Note that this method allows the Fourier plane to be compressed, even if it is impossible to juxtapose the closest pupils, for technical reasons for instance.

2.2 Visibility estimators

There are different ways to recover the individual visibility of each baseline from the recorded image. Before the advent of single-mode interferometry and to overcome the problem of turbulence, Roddier & Lena (1984) developed estimators based on power spectral density (PSD) integration. In Paper I, we exposed the formal expressions of expected values and signal-to-noise ratio (S/N) for this kind of estimator in the framework of filtered multi-axial combiners. In this paper, this method will be called *PSD-integration* (Integ).

It is also possible to measure the visibility by considering only the maximum value of the PSD of each peak. The required calibration is the same as for PSD-integration. This estimator was not specifically studied in the previous paper, but it can be calculated with the same formalism with integration limited to only one pixel (the maximum)

of the Fourier peak. This method will be called *PSD-Maximum* (Max).

By taking more benefit from the deterministic properties of the PSD, the square visibility can be recovered by fitting the PSD shape. The shape has to be previously calibrated by observations of unresolved star or internal light. This estimator was not presented in our previous study. We implemented its theoretical expressions for expected values and the S/N and checked them thanks to numerical experiments described in Paper I. This method will be called *PSD-Fitting* (Fit).

Because the shape of the interferogram is completely determinist, the visibilities can also be recovered by fitting the data. The fit can be identically done in the direct plane (fringe fit) or in the Fourier plane (complex Fourier transform fit). It can be formally expressed as a matricial relation between the recorded values on the detector and the complex visibility of each baseline: the so-called *pixel to visibility matrix* (P2VM). The visibility amplitudes and phases are recovered in the same inversion process. If no fringe tracking unit is available, the phase quantity is stochastic from frame to frame and is meaningless. It is ignored by averaging the square visibility instead of the complex visibility. As a main difference with the PSD-based algorithms presented above (Integ, Max and Fit), this square operation is done *after* the information of the baselines has been separated. The calibration requires the recording of the instrumental fringe shapes with good accuracy. The reader can refer to the AMBER data processing method for which such a model-based algorithm is currently used (Millour et al. 2004).

3 NUMERICAL EXPERIMENT

As far as an astronomer is concerned, the properties of interest when dealing with different estimators are the relative accuracy performance, the relative bias on the expected value and their dependencies with the instrumental parameters.

3.1 Estimator relative performances without compression

Fig. 3 illustrates the performance of the PSD-based estimators compared to the model-based one in different noise regimes, without compression, and for two different detector reading windows ($N_{\rm pattern}$). The source visibility is arbitrarily set to $\mu = 0.5$ and the detector noise is $\sigma = 15\,{\rm e}^-\,{\rm pixel}^{-1}$. The model-based estimator always presents a better S/N, especially in the strong photon-rich and photon-poor domains. The PSD-based estimators follow more or less the same curves for a small detector reading window. However, when increasing the number of independent points over the fringe frequencies ($N_{\rm pattern} > 2$), the PSD-maximum shows a worse performance, because it does not take into account all of the available information. At least, they all reach a similar asymptote in photon-noise limit, from where their S/N is about 0.6 times the model-based one. This asymptote does not depend on the instrumental configuration but is only a function of the source visibility.

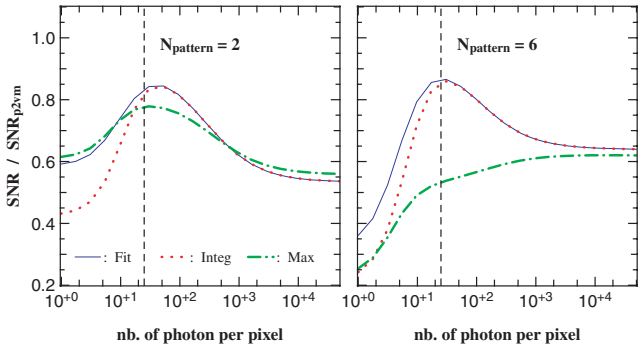

Figure 3. Ratio between the S/N of the PSD-based estimators and the S/N of the model-based one, as a function of the number of photons per pixel in the interferogram. The source visibility is set to $\mu = 0.5$. Detector noise is $\sigma = 15\,{\rm e}^-\,{\rm pixel}^{-1}$. The Fourier peaks are fully separated ($N_{\rm fri} = 2.5$ and no compression). The curves are plotted for a narrow and a large detector reading window (left and right panels).

In Paper I, we have mentioned the advantage of the model-based estimator versus PSD-integration, especially for unresolved sources with high visibility. Showing the computations presented here we conclude that this advantage can be extended over all the PSD-based estimators without exception. It tends to prove that a first-order estimation systematically drives a better (or at worst identical) performance than quadratic one.

3.2 Estimator robustness to compression

To compare the estimator relative robustness to compression, we compute the recovered visibility amplitudes for a large range of compression factors. The initial set-up is the same as in Section 3.1 (four beams, $N_{\rm fri} = 2.5, N_{\rm pattern} = 6$, and pupil positions given by equation 3). For the sake of the clarity of Fig. 4, the input visibilities have been chosen to be arbitrarily different, and all the phases are set to zero. It has absolutely no incidence on the results, which have been validated with various sets of input parameters (combiner geometry, fringe visibilities and phases). Results are displayed in Fig. 4, with a compression factor ranging from 1 to 0.1. As soon as peaks overlap, PSD-integration and PSD-fit rapidly fail to recover to visibility. PSD-maximum only fails when peaks strongly overlap ($\rho \leqslant 0.4$). Besides, the model-based estimation is never biased even when the compression factor reaches 0.1.

The bias in the estimated visibility can be explained by the mixing of information between corresponding peaks when they start to overlap. This blend is due to the coherent sum of the two interferograms under the overlapped frequencies. Because the input phases and optical path delays are arbitrarily zero, the asymptotic square visibility recovered is the square average of the two corresponding 'single' visibilities, as shown in the right asymptotes of Fig. 4. In a general way, it depends on both the visibilities and phases. Such a complex sum prevents a simple calibration of this effect. The only solution is to previously calibrate the complex shape of each individual peak and then to inverse both the amplitudes and the phases at the same time. By doing so, one has just reinvented the model-based estimator in the Fourier space, and it explains why this last estimator is never biased.

3.3 Signal-to-noise ratio versus compression

We now focus on the model-based estimator because we have shown that the latter is the only one able to retrieve unbiased interferometric quantities even if the pupil plane is compressed. Formal expressions of the S/N computed in Paper I remain valid for all compression factors. Computations give similar results in both the photon noise and detector noise regime. We present here only photon-rich computations. The instrumental set-up used is the same as in Section 3.2. Remember that it has been chosen for illustration purpose only and that we checked the results with various combiner configurations.

The right panel of Fig. 4 shows the results, after normalization of the S/N by the value obtained without compression. Three different slopes can be distinguished, as follows.

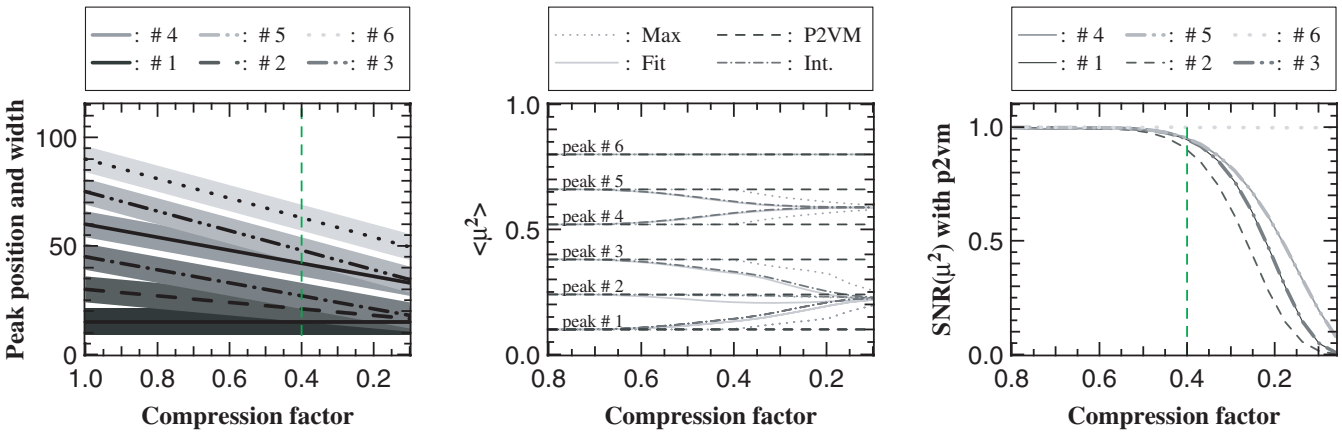

Figure 4. Left panel: positions (thick lines) and supports (filled regions) of the fringe peaks in the Fourier space versus the compression factor. Middle panel: square visibility (μ^2) obtained with the different estimators described in Section 2.2. Right panel: the S/N on the square visibility of each baseline computed for the model-based estimator normalized with respect to the zero-compression factor value ($\rho = 1$). The vertical dashed line is for $\rho = 1/N_{\rm fri} = 0.4$.

(i) Peak 6 never overlaps. Its S/N remains constant.

(ii) Peaks 4 and 5 interact with one neighbour. Their S/N stay unchanged when peaks slightly overlap but rapidly decrease when peaks strongly overlap.

(iii) Peak 2 interacts with its two neighbours. Its S/N stays unchanged for a slight overlap but presents a more abrupt decrease when peaks strongly overlap.

Slopes related to peaks 1 and 3 can be explained as a combination of the latter. They start with two-peak interactions (each of them with a side of peak 2). So their S/N follow the curve of peaks 4 and 5. Then they meet together over peak 2 and begin also to be engaged in a three-peak interaction. Their S/N reach the curve related to peak 2.

The expression of the model-based estimator as a matrix can help to understand these results. Each complex visibility (one per baseline) corresponds to one line of this matrix. When peaks overlap, corresponding lines become more and more similar, and thus singular, which mathematically reduces the accuracy of the inversion. From this study, we conclude that (whatever the initial peak position and the number of neighbours) the S/N is unaffected by a slight overlap but decreases rapidly for a strong one. So a compression factor of $1/N_{\rm fri}$ can be applied to any configuration without damaging the performance, whatever the initial $N_{\rm fri}$ parameter and the noise regime.

3.4 Remarks

In this section, the presented computations have been done with a Gaussian interferogram shape, which is the Fourier transform of a beam filtered by a Gaussian mode. Strictly speaking, a fibre mode is purely Gaussian only if the profile of the refraction index is a Gaussian function too. However, it gives a good approximation in general with step-index fibres or waveguides. All the results have been also checked with a Bessel interferogram envelop (corresponding to circular pupils) and lead to same conclusions. However, one should remember that turbulent beams (not perfectly corrected by adaptive optics or not spatially filtered) will lead to fringes that cannot be fitted by a first-order estimator. Besides, the total number of pixels remains constant in our computations, although it becomes possible to reduce it when the Fourier plane is compressed (Shannon sampling is relaxed). We have tried to optimize the sampling rate for each compression factor, but it does not change the results.

4 APPLICATION TO SIX- AND EIGHT-BEAM COMBINERS

For more than four beams, it is impossible to theoretically determine the best non-redundant pupil configuration P_i that minimizes the maximum frequency used. This well-known problem can only be solved by 'brute force' methods, and non-redundant integer lists have been obtained for a large number of telescopes (Ribak et al. 1988), such as

$$P_i = (0, 1, 4, 10, 12, 17), \tag{5}$$

$$P_i = (0, 1, 8, 20, 22, 25, 31, 35), \tag{6}$$

for six and eight beams, respectively. The maximum of P_i is larger than the number of baselines, even if the configuration is optimized. As a consequence, it leaves gaps in the frequency space. To compress the Fourier plane, we applied equation (4) on the six- and eight-beam configurations. Surprisingly, some peaks fully overlap before the compression factor goes to zero. So we expected that some worse starting P_i configuration (with more gaps) could be more compressed and finally provide a smaller frequency range.

To test it, we directly introduced the minimum allowed overlap rate in the 'brute force' optimization algorithm as a new user-defined parameter ($\rho_{\rm min}$). Fig. 5 shows the results with no compression (top panels, corresponding to equations 5 and 6) and with the maximum overlap rate allowed by our study (bottom panels, $\rho_{\rm min} = 1/N_{\rm fri}$) for six- and eight-beam combiners. There is no simple transformation between the best pupil configurations with and without compression. We infer that it is impossible to find the best compressed configuration from the best uncompressed one. Empirically, we remark that the compact solution leaves more gaps in the frequency space, which are overcompensated by the compression. As a consequence, the maximum frequency is not multiplied by a factor $\rho_{\rm min} = 1/N_{\rm fri} = 0.5$. We only reach a compression of $\sim$0.58 for the six-beam combiner and $\sim$0.55 for the eight-beam combiner.

5 CONCLUSION

In this paper, we have chosen to focus on the multi-axial single-mode interferometry concept because it is one of the most promising solutions for future spectro-imaging interferometers with a large number of telescopes (LeBouquin et al. 2004a). Also, it is currently

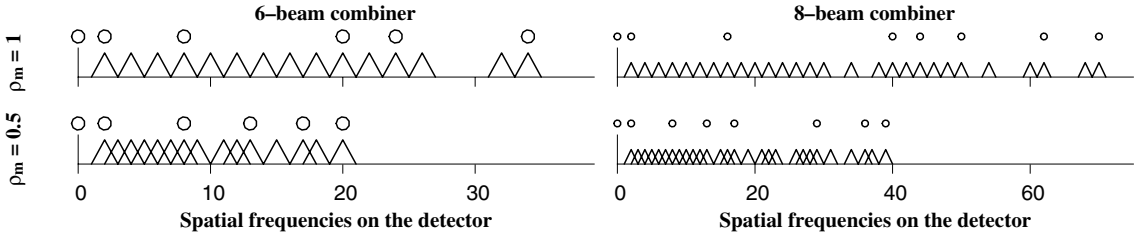

Figure 5. Results of plane optimization for six- (left panels) and eight-beam (right panels) combiners. The output pupil configuration and the Fourier plane are represented at the same scale (autocorrelation relation). The pupil positions are computed for a compression factor of $\rho = 1$ (top panels) and $\rho = 0.5$ (bottom panels). The minimum distance between the pupils is set to twice the pupil width ($N_{\rm fri} = 2$). The frequency range is reduced by a factor 0.58 and 0.55 in the six- and eight-beam cases, respectively.

used in the AMBER instrument. Based on this specific recombination scheme, we have proposed a simple method by compressing the output pupil plane by keeping a partial non-redundancy condition. We then have recalled the definition of four different visibility estimators that can be classified into two types: the estimators that make use of the PSD of the interferogram and the estimator based on the model fitting of the interferogram.

First extending our analysis of Paper I, we have shown that without compression, the model-based estimator drives to better performances than all PSD-based estimators, whatever the noise regime (detector or photon noise) and the instrumental set-up. This tends to prove that a first-order estimation systematically drives a better performance than a quadratic one. Then we have analysed the effects of compression on these estimators. We have demonstrated that a model-based estimator is as well the suitable algorithm to deal with compression. Indeed, by first separating the baseline complex visibilities before taking the modulus, the method prevents information mixing between the baselines that leads to a bias in the visibility. Yet, the compression reduces the S/N because the matrix used in the inversion process becomes more and more singular. However, the accuracy on the visibilities is not dramatically damaged before the peak maximum reaches the edge of its close neighbour, which we have called a slight overlap.

With regard to the existing AMBER instrument, this study allows us to claim that the model-based estimator (the so-called P2VM, Millour et al. 2004) is a suitable algorithm and that the pupil overlap rate used (slight overlap) only reduces the S/N by a few per cent.

With regard to future instruments dealing with a larger number of input beams, we propose to use this overlapping rate to minimize the required frequency range. None the less, we have shown that the maximum frequency can be multiplied by a factor smaller than 0.6. Such an optimization of the output pupil configuration has important consequences. First, it reduces the number of pixels per spectral channel, leading to a smaller contribution of the detector noise and a better limiting magnitude. Secondly, it reduces the minimum required spectral resolution and thus increases again the limiting magnitude when dispersion is not mandatory for the scientific case. At the same time, by reducing the number of required pixels and/or spectral channels, it increases the reading speed, which is an important parameter if no fringe tracking unit is available.

From a technical point of view, integrated optics (IO) offers promising solutions to realize a multi-axial single-mode combiner. This technology has been proved with both laboratory and sky experiments (Berger et al. 2001; LeBouquin et al. 2004b), and multi-axial combiners have already been designed (Berger et al. 2000). The size of the chip is directly related to the physical space between the output pupils. Because losses are mainly due to linear propagation in the waveguides, reducing the required distance between the beams, as presented in this work, will lead to a better global efficiency. The compactness of the planar optical component allows one to combine many beams in the same chip, which drastically reduces the instability and the required alignments. The observational strategies (number of baselines, wavelength. . .) can be adapted to the object thanks to the plug and play ability of IO combiners. Finally, output beams of the planar component can act as the input slit of a spectrograph, avoiding complex anamorphic optics.

ACKNOWLEDGMENTS

The authors want to warmly thank Florentin Milour, Karine Perraut, Jean-Philippe Berger and Fabien Malbet for their interesting remarks and help. We are grateful for the valuable comments by the referee, which helped to improve this article. All the calculations and graphics were performed with the freeware YORICK.[1]

REFERENCES

Baldwin J. E. et al., 1996, A&A, 306, L13
Berger J., Benech P., Schanen-Duport I., Maury G., Malbet F., Reynaud F., 2000, in Lena P. J., Quirrenbach A., eds, Proc. SPIE Vol. 4006, Interferometry in Optical Astronomy. SPIE Publishing, Bellingham, p. 986
Berger J. P. et al., 2001, A&A, 376, L31
Coudé Du Foresto V., Perrin G. S., Ruilier C., Mennesson B. P., Traub W. A., Lacasse M. G., 1998, in Reasenberg R. D., ed., Proc. SPIE Vol. 3350, Astronomical Interferometry. SPIE Publishing, Bellingham, p. 856
Glindemann A. et al., 2003, in Traub W. A., ed., Pro. SPIE Vol. 4838, Interferometry for Optical Astronomy II. SPIE Publishing, Bellingham, p. 89
Hummel C. A., 1998, in Reasenberg R. D., ed., Proc. SPIE Vol. 3350, Astronomical Interferometry. SPIE Publishing, Bellingham, p. 483
LeBouquin J.-B., Berger J., Labeye P., Tatulli E., Malbet F., Rousselet-Perraut K., Kern P. Y., 2004a, in Traub W. A., ed., Proc. SPIE Vol. 5491, New Frontiers in Stellar Interferometry. SPIE Publishing, Bellingham, p. 1362
LeBouquin J.-B. et al., 2004b, A&A, 424, 719
Malbet F. et al., 2004, in Traub W. A., ed., Proc. SPIE Vol. 5491, New Frontiers in Stellar Interferometry. SPIE Publishing, Bellingham, p. 439
Mège P., 2003, PhD thesis, Univ. Joseph Fourier de Grenoble
Millour F., Tatulli E., Chelli A., Duvert G., Zins G., Acke B., Malbet F., 2004, in Traub W. A., ed., Proc. SPIE Vol. 5491, New Frontiers in Stellar Interferometry. SPIE Publishing, Bellingham, p. 1222

[1] http://yorick.sourceforge.net/index.php

Monnier J. D., Berger J.-P., Millan-Gabet R., Ten Brummelaar T. A., 2004a, in Traub W. A., ed., Proc. SPIE Vol. 5491, New Frontiers in Stellar Interferometry. SPIE Publishing, Bellingham, p. 1370
Monnier J. D. et al., 2004b, ApJ, 602, L57
Perrin G., 1997, A&AS, 121, 553
Petrov R. G. et al., 2003, in Traub W. A., ed., Proc. SPIE Vol. 4838, Interferometry for Optical Astronomy II. SPIE Publishing, Bellingham, p. 924
Ribak E. N., Hochberg E. B., Page N. A., Synnott S. P., Breckinridge J. B., 1988, in F. Merkle, ed., ESO Conf. and Workshop Proc. No. 29, NOAO-ESO Conference on High-Resolution Imaging by Interferometry: Ground-Based Interferometry at Visible and Infrared Wavelengths. ESO, Garching, p. 1105
Roddier F., Lena P., 1984, J. Opt., 15, 363
Tatulli E., LeBouquin J.-B., 2006, MNRAS, 368, 1159 (Paper I)
Tatulli E., Mége P., Chelli A., 2004, A&A, 418, 1179
Thiébaut E., Garcia P. J. V., Foy R., 2003, Astrophys. Space Sci., 286, 171
Vakili F., Koechlin L., 1989, in Swings J.-P., ed., Proc. SPIE Vol. 1130, New technologies for astronomy. SPIE Publishing, Bellingham, p. 109
Young J. S. et al., 2000, MNRAS, 315, 635

This paper has been typeset from a TEX/LATEX file prepared by the author.